physica status solidi

pss

www.pss-journals.com

reprint

WILEY-VCH

Phys. Status Solidi C **11**, No. 5–6, 1074–1079 (2014) / **DOI** 10.1002/pssc.201300699

physica status solidi c
www.pss-c.com
current topics in solid state physics

Exchange coupling and magnetic anisotropy for different concentration of iron based nanoparticles in aligned carbon nanotube arrays

Serghej L. Prischepa[*,1], Alexander L. Danilyuk[1], Alena L. Prudnikava[1], Ivan V. Komissarov[1], Vladimir A. Labunov[1], and Francois Le Normand[2]

[1] Belarusian State University of Informatics and Radioelectronics, P. Brovka str. 6, 220013 Minsk, Belarus
[2] Laboratory of Engineering, Informatics and Imagery (ICube), Département Electronique des Solides, des Systèmes et de Photonique (DESSP), Université de Strasbourg and CNRS, Bat. 28, 23 Rue du Loess, BP 20 CR, 67037 Strasbourg Cedex 2, France

Received 24 October 2013, revised 17 January 2014, accepted 3 February 2014
Published online 17 April 2014

Keywords magnetic nanocomposite, carbon nanotube, exchange coupling, magnetic anisotropy, magnetic nanoparticle

[*] Corresponding author: e-mail prischepa@bsuir.by, Phone: +375-17-2932317, Fax: +375-17-2932356

We present results of study of magnetic properties of nanocomposite formed *in situ* during the synthesis of aligned carbon nanotube (CNT) arrays. CNTs were grown by the atmospheric pressure floating catalyst chemical vapor deposition method. High temperature pyrolysis of ferrocene/xylene solution injected into the quartz tube at high temperature was carried out. By varying the ferrocene content (C_F) in the ferrocene/xylene solution we tuned the concentration, location, size, shape and chemical state of iron based catalytic ferromagnetic nanoparticles. The variation of these parameters was reflected in the magnetic properties of the CNT based nanocomposite. In particular, it is shown, that the main interaction mechanism between ferromagnetic nanoparticles for high C_F contents is the exchange coupling, while the magnetic anisotropy dominates at low ferrocene concentration. The role of the orientation of the nanotubes is decisive for the observation of magnetic anisotropy. When the alignment is destroyed, the exchange coupling mechanism starts to dominate also for low C_F samples.

1 Introduction Properties of magnetic nanocomposites are intensively studied during last years [1]. New functionalities are obtained when combining a favorable matrix and filler properties [2]. However, it is still very important to understand the nature of magnetic interaction between nanoparticles and possible role of matrix which could influence the strength of this coupling.

In particular, when the average distance between nanoparticles is in the nanometric range, the exchange interaction could dominate. At that the magnetic anisotropy of each nanoparticle should also be taken into account thus creating very complicated picture of interparticle interaction. The matrix material could also induce the additional difficulties in the experimental data interpretation. For example, for a nanocomposite consisting of carbon nanotubes (CNTs) with intercalated magnetic nanoparticles, the CNT alignment and/or possible indirect exchange coupling [3] could significantly modify the nanocomposite properties with respect to other matrix materials, like polymers [2], silica [4], porous silicon [5], etc.

Generally, magnetic nanoparticles smaller than 30 nm could be prepared by different methods, such as co-precipitation, thermal decomposition, emulsion method, hydrothermal synthesis [6], co-evaporation, co-sputtering [2], laser ablation in liquid [7], etc. On the other hand, it is necessary to precisely control the chemical stoichiometry of the nanoparticles in the nanocomposite, their sizes and shape, as well as the average distance between them.

From this viewpoint CNT based magnetic nanocomposites are very promising. Generally, CNTs are synthesized involving carbon decomposition of organic precursor over $3d$ catalytic metals like Fe, Ni, and Co [8]. At that the ferromagnetic catalytic nanoparticles could be intercalated over the whole volume of the sample and the magnetic CNT based nanocomposite is synthesized *in situ*, during the CNTs growth. It is possible to produce aligned and macroscopically large CNT arrays filled with ferromagnetic nanoparticles of different morphology and phase content [9,10]. Moreover, the ferromagnetic inclusions are covered by carbon shell thus preventing oxidation and accordingly some antiferromagnetic contribution [11]. Therefore, such CNT based nanocomposites possess high temperature stability. The coercivity of these nanocomposites is much larger with respect to bulk ferromagnets, reaching the values of thousands of Oersteds [12].

Recently we have reported the magnetic properties of CNT based nanocomposites paying special attention on the interplay between exchange interaction and magnetic anisotropy for iron based nanoparticles intercalated into CNT array [13]. In particular, we have shown that the correlation between the concentration and location of the ferromagnetic catalytic nanoparticles in CNT based nanocomposites and their magnetic properties does exist. In this work we continue to develop the approach proposed in [13]. In particular, we analyze in details the correlation functions of the magnetic anisotropy axes which describe the magnetic state of iron based nanoparticles in CNT array and we explicitly show the dependence of the deduced correlation functions on such important technological parameter as the ferrocene content C_F in ferrocene/xylene solution during the floating catalyst chemical vapor deposition (CVD).

2 Experimental Floating catalyst CVD was used for the synthesis of CNT based nanocomposite on Si substrates. Three concentrations of ferrocene $Fe(C_5H_5)_2$, $C_F = 0.5$ wt%, 1 wt% and 10 wt%, respectively, were used. The temperature in the reaction zone was fixed to 1150 K and the growth duration was 1 min. This created vertically-aligned multiwalled CNT arrays of typical thickness of 70 μm with CNT diameter of $10-30$ nm. Catalytic iron based nanoparticles are mainly located in the inner channels of CNTs for $C_F = 0.5\%$, and are distributed also inside and outside walls for larger C_F values. The average size of nanoparticles varied in the range $\sim 10-30$ nm depending on the ferrocene content during the synthesis [14]. The concentration of the nanoparticles for $C_F = 10\%$ was much higher than for samples synthesized with $C_F = 0.5\%$. At that the major ferromagnetic phases of iron based nanoparticles are α-Fe and cementite Fe_3C [10]. Mössbauer spectroscopy revealed that the content of the Fe_3C is increased with C_F growth. For $C_F = 10\%$ it reached the value of 80%. Reversely, content of α-Fe phase dropped with C_F, and for $C_F = 10\%$ it becomes less than 15% [10]. More details about the sample preparation and characterization could be found elsewhere [14, 15].

Magnetic properties were studied by measuring the zero filed cooled (ZFC) and field cooled (FC) magnetizations at $H = 75$ Oe as a function of temperature, as well as isothermal magnetic hysteresis loops, $M(H)$, at a given temperature using a MPMS SQUID-VSM magnetometer (Quantum Design). The magnetic field was varied in the range from -7 T to $+7$ T, within the temperature interval 2 K-380 K. The magnetic moment was measured with the sensitivity of 10^{-8} emu. The magnetic field was always applied parallel to the CNT axis, i.e. perpendicular to the surface substrate.

For the elaboration of the magnetic data the exact mass of the ferromagnetic content was necessary to be known. For that we used the atomic absorption spectroscopy, which allowed obtaining the iron mass with a precision less than 0.01%.

3 Results and discussion

3.1 Magnetostatic parameters In Fig. 1 the ZFC-FC magnetizations versus temperature for aligned samples synthesized with $C_F = 0.5\%$ (dashed lines) and $C_F = 10\%$ (solid lines) are shown. It is clearly seen that curves only coincide at the highest temperature measured. Therefore the blocking temperature (T_B) is set close above these values. Nevertheless, it is possible to extract useful qualitative information from the analysis of these data. In particular, a near flat FC curve for the sample with $C_F = 10\%$ indicates strong interaction of nanoparticles, while the absence of such strength of the interparticle interaction for the sample with $C_F = 0.5\%$ is evident. This is due to much lower concentration of nanoparticles in the last case [14].

The magnetization curves, measured for the aligned sample with $C_F = 1\%$ at different temperatures are shown in Fig. 2. The ferromagnetic order presents up to the maximum temperature, at which measurements were performed, $T = 380\ K$. The evolution of the symmetric magnetic hysteresis loops shows a narrowing tendency towards higher temperatures. Similar results were obtained for samples synthesized with $C_F = 0.5\%$ and 10%.

Three main magnetostatic parameters can be extracted from the isothermal hysteresis magnetization curves, the saturation magnetization M_{sat}, the coercivity H_C and the remanence M_{rem}. Moreover, the performed $M(H)$ measurements of samples synthesized with different C_F contents at different temperatures allowed studying both the temperature T and ferrocene concentration C_F dependencies of the obtained parameters. In Fig. 3 we present the squareness (M_{rem}/M_{sat}) of the $M(H)$ loops versus C_F at three temperatures, $T = 2$ K, 150 K and 300 K. Analysis of results of Fig. 3 indicates that the squareness initially increases with C_F, and then it flattens out. For $C_F = 10\%$ the squareness at $T = 300\ K$ becomes less than for $C_F = 1\%$. For $T = 2$ K and $T = 150$ K the squareness

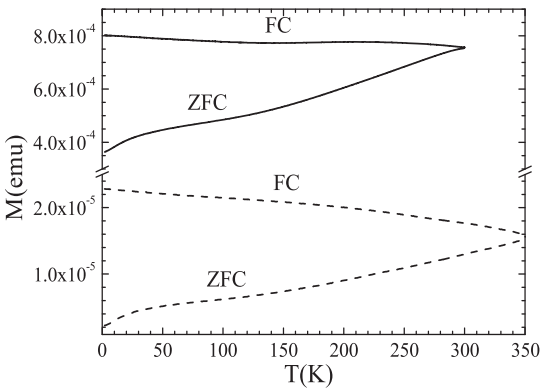

Figure 1 ZFC and FC magnetizations versus temperature for aligned samples synthesized with $C_F = 0.5\%$ (dashed lines) and $C_F = 10\%$ (solid lines).

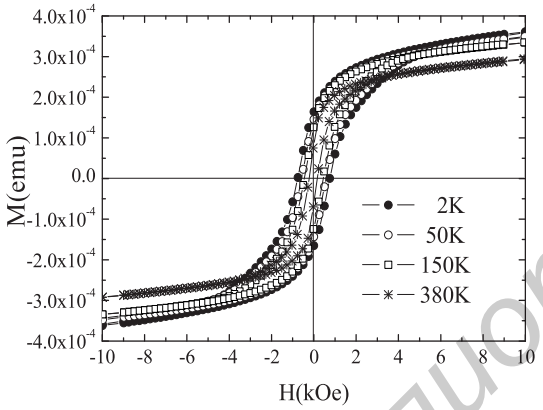

Figure 2 Magnetization versus magnetic field for the aligned sample synthesized with $C_F = 1\%$ at 4 different temperatures.

between $C_F = 1\%$ and 10% practically does not change. For $C_F = 0.5\%$, however, it clearly drops for all temperatures. This indicates that ferromagnetic nanoparticles in the sample synthesized with $C_F = 0.5\%$ are scattered and less interacting. This is in good agreement with the result of the ZFC-FC magnetizations, as reported in Fig.1. The decrease of the squareness at high temperature values could be due to thermal fluctuations. The coercivity also increases with C_F [13]. It is mostly due to the increase of the average size of the nanoparticles with the ferrocene content.

3.2 Random anisotropy model (RAM) and micromagnetic parameters On the basis of the obtained experimental data one can try to clarify the mechanism of magnetic interparticle coupling in our samples. In order to distinguish whether ferromagnetic nanoparticles are coupled via the exchange interaction, or their anisotropy energy is enough to compete the interparticle exchange coupling, we consider here the random anisotropy model (RAM) [16–18]. The RAM has been successfully applied in the past to explain the properties of amorphous [19] and nanocrystalline ferromagnets [20], as well as Fe_3C nanoparticles in CNTs [21]. Within the RAM it is possible to evaluate important micromagnetic parameters, such as the effective magnetic anisotropy K_{eff}, the anisotropy field H_a, the exchange field H_{ex} and the constant of the exchange coupling of the ferromagnetic material A. The key to the RAM is the assumption of the presence of chaos in the direction of the local magnetic anisotropy and the possibility of describing the magnetic structure of a set of weakly coupled magnetic blocks of size of ferromagnetic correlation length R_F [22]. The anisotropy field H_a and the exchange field H_{ex} are expressed as $H_a = 2K_{eff}/M_{sat}$ and $H_{ex} = 2A/M_{sat}R_a^2$, respectively. Here R_a is the length over which the magnetic anisotropy axes are correlated. Usually in a nanocrystalline material R_a is assumed to be equal to the radius of the nanoparticle, R_n [20]. Actually the value of R_F is expressed as $R_F \approx R_a(H_{ex}/H_a)^2$ [23]. The exchange coupling constant A could be calculated according to the relation $A = (\frac{k_B}{8\pi})(\frac{M_{sat}}{g\mu_B})^{1/3}(\frac{2.612}{B})^{2/3}$ [24], where g is the Landé splitting factor, k_B is the Boltzmann constant, μ_B is the Bohr magneton and B is the Bloch's constant. The latter value was obtained from the analysis of the temperature dependence of the saturation magnetization [13] according to the Bloch's law, $M_{sat}(T) = M(0)(1-BT^{3/2})$. The average radius R_n of the ferromagnetic nanoparticles in the assumption of a spherical form was calculated according to the standard relation $R_n = (\frac{3}{4\pi}25\frac{k_BT_B}{K_{eff}})^{1/3}$. The T_B values were obtained from the temperature dependencies of the coercivity, $H_C(T)$, as described in [25].

The coercivity in the RAM is expressed as [17]

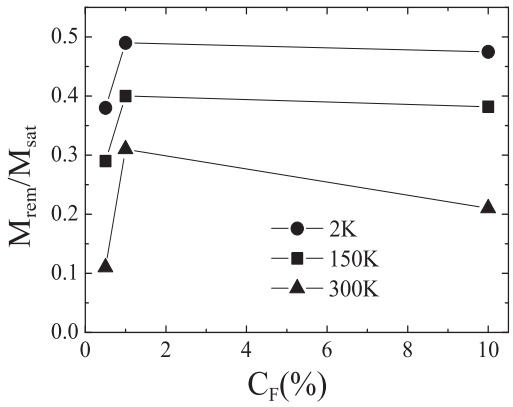

Figure 3 The squareness (M_{rem}/M_{sat}) of the $M(H)$ loops versus the ferrocene content C_F at different temperatures.

$$H_C \approx \frac{3.2 R_n^6 K_{eff}^4}{A^3 M_{sat}}. \quad (1)$$

Combining the formula for R_n and Eq. (1) we arrive to the expression for the effective anisotropy constant,

$$K_{eff}^2 = \frac{H_C A^3 M_{sat}}{114 (k_B T_B)^2}. \quad (2)$$

Therefore, H_{ex}, H_a and K_{eff} values of the nanocomposite can be evaluated from such measurable quantities as H_C, M_{sat}, T_B and B. In particular, for the sample synthesized with $C_F = 0.5\%$ we obtained the following set of micromagnetic parameters, $K_{eff} = 1.76 \times 10^4$ J/m^3, $H_{ex} = 5.73$ kOe, $H_a = 2.73$ kOe. For the sample synthesized with $C_F = 1\%$ we got $K_{eff} = 1.25 \times 10^4$ J/m^3, $H_{ex} = 2.88$ kOe, $H_a = 2.1$ kOe. And for the sample with $C_F = 10\%$ the parameters were $K_{eff} = 0.6 \times 10^4$ J/m^3, $H_{ex} = 2.52$ kOe, $H_a = 2.0$ kOe. All these data are for $T = 50$ K.

3.3 Law of the approach to saturation (LAS) and correlation functions To verify the physical meaning of the obtained micromagnetic parameters we analyzed the magnetization in the approach to saturation ($H > 1$ kOe). Analyzing the law of the approach to saturation (LAS) it is possible not only to check the micromagnetic parameters of the nanocomposite, but also to obtain useful information regarding the correlation in the orientation of the magnetic anisotropy axes of nanoparticles in real space [26]. Generally the LAS is expressed as [18]

$$\frac{\delta M}{M_{sat}} = \frac{M_{sat} - M(H)}{M_{sat}} \sim H^{\alpha}, \quad (3)$$

where the exponent α depends on the relation between H and H_{ex}. For $H \ll H_{ex}$ the exponent is $\alpha = -1/2$, while for $H \gg H_{ex}$ it is $\alpha = -2$ [23].

In Fig. 4 we plot the high field part of the magnetization loops, according to the Eq. (3), for aligned samples synthesized with $C_F = 0.5\%$ (Fig. 4a) and 1% (Fig. 4b). Data are for $T = 50\ K$. It is seen the drastic change of the exponent α with small variations of C_F. Indeed, it was found that the experimental dependence for the sample synthesized with $C_F = 0.5\%$ is described by Eq. (3) only if the exponent is $\alpha = -2$ (Fig. 4a). While for samples synthesized with $C_F = 1\%$ and 10% the exponent is $\alpha = -1/2$, which means $\delta M/M_{sat} \sim H^{-1/2}$. Moreover, the obtained LAS are valid for the sample with $C_F = 0.5\%$ in the field range $3 - 7\ kOe$, which covers the value of the exchange field for this sample $H_{ex} = 5.73$ kOe (the dashed vertical line in Fig. 4a). For the sample synthesized with $C_F = 1\%$ the LAS with the exponent $\alpha = -1/2$ is valid in the range $1 - 7$ kOe, which also spans the value of $H_{ex} = 2.88\ kOe$ (the dashed vertical line in Fig. 4b).

In the case when the experimental range of H crosses the H_{ex} value, analysis of the LAS should be done within the more general expression [22,23,27]

$$\frac{M(H)}{M_{sat}} = 1 - \frac{\lambda^2}{30 p(H)} \int_0^{\infty} d^3 r \; exp\left[-p(H) r\right] r^2 \; C(r) \quad (4)$$

with $p^2 = H/H_{ex}, r = x/R_a, \lambda = (2/15)^{1/2}(K_{eff}/A)R_a^2$ and x as a coordinate. $C(r)$ is a correlation function describing the distance over which the magnetic anisotropy axes are correlated, scaled with $C(r = 0) = 1$ and $C(r \gg 1) = 0$ [20,27]. Correlation function is determined using the inverse Laplace transform of the Eq. (4).

The analysis performed according to the Eq. (4) revealed that, the correlation function for the aligned sample synthesizes with $C_F = 0.5\%$ is Fermi-Dirac-like function

$$C(r) = \frac{1}{1 + exp\left(\frac{r - r_{1/2}}{2}\right)}, \quad (5)$$

where $r_{1/2}$ is a coordinate at which the value of the correlation function is equal to 1/2.

This result is shown in Fig. 5 by the solid line. The correlation of the magnetic anisotropy axes is present on macroscopically large distance, up to hundreds of nanometers. According to our opinion, this is the influence of the CNT alignment. Indeed, such obtained extended order means the absence of the dominant role of random anisotropy in this sample ($C_F = 0.5\%$). On the other hand, the observed LAS of the type $\delta M/M_{sat} \sim H^{-2}$ usually is associated with the magnetization of uncoupled single domain nanoparticles, for which the exchange interaction is negligibly small [28]. Therefore, it is reasonable to assume that for sample, synthesized with low ferrocene concentration, for which all the ferromagnetic nanoparticles are localized inside the inner channels of CNTs [14], the CNT alignment could reinforce the coherent (i.e. non random) magnetic anisotropy, which usually is much weaker than the random one [18]. In other words, the CNT alignment together with the ferromagnetic nanoparticles localization in the inner CNT channels facilitates the appearance of the orientational order in the sample.

The importance of the CNT alignment on the extended orientational order was proved directly by studying the LAS for a powder formed from the aligned sample synthesized with $C_F = 0.5\%$. For powder the alignment is destroyed and sample consists of randomly oriented blocks. Inside each block CNTs are aligned, but the entire sample consists of misaligned nanotubes. The high field part of the magnetization curve plotted according to the Eq. (3) for the powder formed from the aligned sample with $C_F = 0.5\%$ is shown in Fig. 4b by squares. It is clearly seen that the experimental data are described according to the Eq. (3),

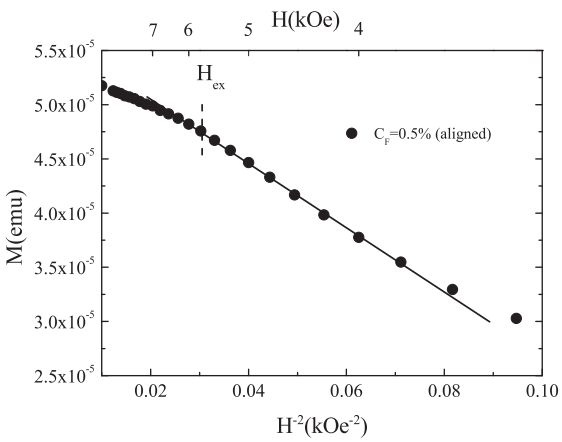

a) Aligned sample synthesized with $C_F = 0.5\%$.

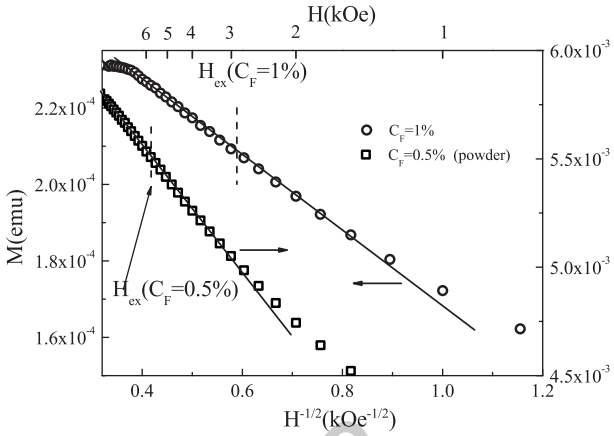

b) Aligned sample synthesized with $C_F = 1\%$ (circles). Powder fabricated from the aligned sample synthesized with $C_F = 0.5\%$ (squares).

Figure 4 Analysis of the LAS according to the Eq. (3). Data are for $T = 50\ K$. Solid lines are for the best fit results for each data. Vertical dashed lines indicate the H_{ex} values. The range of the magnetic field in which the LAS according to the Eq. (3) is satisfied can be estimated from the upper horizontal axis of the figure.

but with the exponent $\alpha = -1/2$ instead of $\alpha = -2$, as it was for the aligned sample (see Fig. 4a).

Correlation functions for samples of aligned CNT synthesized with $C_F = 1\%$ and 10% differ significantly from that for the sample with $C_F = 0.5\%$. The performed on the base of Eq. (4) analysis revealed that the correlation function for these samples is Bessel function of the first kind

$$C(r) = \beta^{-1/2} r^{\frac{\nu-4}{2}} J_\nu(2\beta^{1/2} r^{1/2}), \qquad (6)$$

where β and ν are constants. This function decays rapidly on distance of a few nanometers, which means the rapid decrease of the magnetic anisotropy contribution and increase of the exchange interaction between nanoparticles. As an example, in Fig. 5 we show the correlation function for the sample synthesized with $C_F = 1\%$ (dashed line). The same type of the correlation function was also obtained for the aligned sample with $C_F = 10\%$ and for the powder formed from the aligned CNTs with $C_F = 0.5\%$. The result for the powder is shown in Fig. 5 by the dotted line. The weak oscillating character of the obtained correlation functions does not mean the oscillation of the magnetic anisotropy. According to our opinion, it could be mostly caused by the peculiarities in the exchange interparticle interaction and influence of the CNT matrix on it. Indeed, the indirect exchange coupling characterizes the carbon nanotubes [3]. This could cause the oscillating character of the exchange coupling, which reflects in the weakening and strengthening of the magnetic anisotropy contribution along the CNT. But this mechanism is absent in the RAM which has been applied for the discussion of the experimental data.

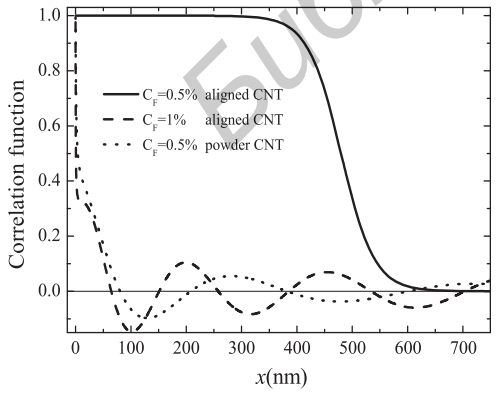

Figure 5 Correlation functions for aligned samples synthesized with $C_F = 0.5\%$ (solid line), and 1% (dashed line) and the correlation function for the powder obtained from the aligned sample synthesized with $C_F = 0.5\%$ (dotted line).

4 Conclusions The relation between the exchange interaction and magnetic anisotropy for different concentration of iron based nanoparticles in aligned carbon nanotube arrays has been studied. Samples have been obtained *in situ* during the floating catalyst CVD. The analysis of the experimental data showed that the LAS is proportional

to the ratio $(\frac{H}{H_{ex}})^{-2}$ for $C_F = 0.5\%$. When $C_F \geq 1\%$ the obtained LAS is proportional to $(\frac{H}{H_{ex}})^{-1/2}$. Moreover, the obtained values of the exchange field are always in the range where the observed laws of the approach to saturation are valid. This fact entails finding the correlation functions that determine the contribution of the random anisotropy. It is shown that, for $C_F = 0.5\%$ the correlation function is stepwise (the step length is around 500 nm) and is described by the Fermi-Dirac function. In this case the exchange interaction between magnetic nanoparticles is weak and the main contribution to the energy makes the random and coherent anisotropy. This effect is caused by the fact that the CNT alignment together with the ferromagnetic nanoparticles localization in the inner CNT channels facilitates the appearance of the orientational order in the sample.

For aligned samples synthesized with $C_F \geq 1\%$ as well as for disaligned samples with $C_F = 0.5\%$ the correlation function decays rapidly, is oscillatory and is described by the Bessel function of the first kind. In this case the main mechanism of the interparticle interaction becomes the exchange coupling. It could be caused by the indirect exchange coupling which is characteristic of carbon nanotubes and reflects the competition between the exchange and anisotropy interactions of iron based nanoparticles in CNT arrays.

Acknowledgements Authors acknowledge the financial support from the European Community's Seventh Framework Programme (FP7/2007-2013) under Grant No. 295016 (BELERA). Partial financial support from the Belarusian Foundation for Basic Research, grant No. F13F-002, is also acknowledged.

References

[1] S. Behrens, Nanoscale **3**, 877 (2011).
[2] F. Faupel, V. Zaporojtchenko, T. Strunkus, and M. Elbahri, Adv. Eng. Mater. **21**, 1177 (2010).
[3] A.T. Costa Jr., D.F. Kirwan, and M.S. Ferreira, Phys. Rev. B **72**, 085402 (2005).
[4] S. Laurent, D. Forge, M. Port, A. Roch, C. Robic, L.V. Els, and R.N. Muller, Chem. Rev. **108**, 2064 (2008).
[5] A.L. Dolgiy, S.V. Redko, I. Komissarov, V.P. Bondarenko, K.I. Yanushkevich, and S.L. Prischepa, Thin Solid Films **543**, 133 (2013).
[6] J. Liu, S.Z. Qiao, Q.H. Hu, and G.Q. (Max) Lu, Small **7**, 425 (2011).
[7] N. Tarasenka, A. Butsen, V. Pankov, and N. Tarasenko, Phys. Status Solidi B **250**, 809 (2013).
[8] V. Jourdain and C. Bichara, Carbon **58**, 2 (2013).
[9] F. Banhart, N. Grobert, M. Terrones, J.C. Charlier, and P.M. Ajayan, Int. J. Mod. Phys. B **15**, 4037 (2001).
[10] A.L. Prudnikava, J.A. Fedotova, J.V. Kasiuk, B.G Shulitski, and V.A Labunov, Semic. Phys. Quantum Electron. Optoelectron. **13**, 125 (2010).
[11] C.T. Fleaca, I. Morjan, R. Alexandrescu, F. Dimitrache, I. Soare, L. Gavrila-Florescu, F. Le Normand, and A. Derory, Appl. Surf. Sci. **255**, 5386 (2009).
[12] F.C. Dillon, A. Bajpai, A. Koos, S. Downes, Z Aslam, and N. Grobert, Carbon **50**, 3674 (2012).
[13] A.L. Danilyuk, A.L. Prudnikava, I.V. Komissarov, K.I. Yanushkevich, A. Derory, F. Le Normand, V.A. Labunov, and S.L. Prischepa, Carbon **68**, 337 (2014).
[14] V. Labunov, A. Prudnikava, K. Yanushkevich, A. Basaev, A. Danilyuk, Y. Fedotova, and B. Shulitski, in: Carbon Nanotubes: Applications on Electronic Devices, edited by J.M. Marulanda (InTech, 2011).
[15] V.A. Labunov, A.L. Danilyuk, A.L. Prudnikava, I. Komissarov, B.G. Shulitski, C. Speisser, F. Antoni, F. Le Normand, and S.L. Prischepa, J. Appl. Phys. **112**, 024302 (2012).
[16] R. Harris, M. Plischke, and M.J. Zuckerman, Phys. Rev. Lett. **31**, 160 (1973).
[17] R. Alben, J.J. Becker, and M.C. Chi, J. Appl. Phys. **49**, 1653 (1978).
[18] E.M. Chudnovsky, W.M. Saslow, and R.A. Serota, Phys. Rev. B **33**, 251 (1986).
[19] J. Tejada, B. Martinez, A. Labarta, R. Grössinger, H. Sassik, M. Vazguez, and A. Hernando, Phys. Rev. B **42**, 898 (1990).
[20] J.F. Löffler, J.P Meier, B. Doudin, J.-P. Ansermet, and W. Wagner, Phys. Rev. B **57**, 2915 (1998).
[21] S.V. Komogortsev, R.S Iskhakov, A.D Balaev, A.G. Kudashov, A.V Okotrub, and S.I Smirnov, Phys. Solid State **49**, 734 (2007).
[22] E.M. Chudnovsky, J. Appl. Phys. **64**, 5770 (1988).
[23] E.M. Chudnovsky, J. Magn. Magn. Mater. **79**, 127 (1989).
[24] F. Keffer, Spin Waves, in: Handbuch der Physik, Vol. 18/2 (Springer-Verlag, Berlin, 1966).
[25] J.L. Dormann, D. Fiorani, and E. Tronc, Adv. Chem. Phys. **98**, 283 (1997).
[26] J. Tejada, B. Martinez, A. Labarta, and E.M. Chudnovsky, Phys. Rev. B **44**, 7698 (1991).
[27] E.M. Chudnovsky and J. Tejada, Europhys. Lett. **23**, 517 (1993).
[28] R.S. Iskhakov, S.V. Komogortsev, A.D. Balaev, and L.A. Chekanova, JETP Lett. **72**, 304 (2000).